326 *Macromolecules* **2010**, *43*, 326–333
DOI: 10.1021/ma901950u

Macromolecules
ARTICLE

# $CO_2$-Philic Polymer Membrane with Extremely High Separation Performance

**Wilfredo Yave,*[,†,§] Anja Car,[†,§] Sergio S. Funari,[‡] Suzana P. Nunes,[†,∥] and Klaus-Viktor Peinemann[†,∥]**

[†]*Institute of Polymer Research and Institute of Materials Research, GKSS Research Centre Geesthacht GmbH, Max-Planck-Str. 1, 21502 Geesthacht, Germany, and* [‡]*Hasylab at DESY, Notkerstr. 85, 22603 Hamburg, Germany.* [§]*Present address: Institute of Materials Research, GKSS-Research Centre Geesthacht GmbH.* [∥]*Present address: 4700 KAUST, Thuwal 23955-6900, Saudi Arabia.*

*Received September 2, 2009; Revised Manuscript Received October 14, 2009*

ABSTRACT: Polymeric membranes are attractive for $CO_2$ separation and concentration from different gas streams because of their versatility and energy efficiency; they can compete with, and they may even replace, traditional absorption processes. Here we describe a simple and powerful method for developing nanostructured and $CO_2$-philic polymer membranes for $CO_2$ separation. A poly(ethylene oxide)−poly(butylene terephthalate) multiblock copolymer is used as membrane material. Smart additives such as polyethylene glycol dibutyl ether are incorporated as spacers or fillers for producing nanostructured materials. The addition of these specific additives produces $CO_2$-philic membranes and increases the $CO_2$ permeability (750 barrer) up to five-fold without the loss of selectivity. The membranes present outstanding performance for $CO_2$ separation, and the measured $CO_2$ flux is extremely high ($> 2\ m^3\ m^{-2}\ h^{-1}\ bar^{-1}$) with selectivity over $H_2$ and $N_2$ of 10 and 40, respectively, making them attractive for $CO_2$ capture.

## Introduction

Global warming is mainly caused by the combustion of fossil fuels and other human activities, leading to carbon dioxide ($CO_2$) emissions. $CO_2$ sequestration is therefore needed [1], and because $CO_2$ is always in a mixture of gases, an efficient separation technology is also required.

The development of innovative materials, which efficiently separate $CO_2$ from other gases, is a big task in the membrane field. Nanotechnology might help us to master this challenge. Ethylene oxide (EO) containing block copolymers or, more generally, polyethers have been identified as outstanding $CO_2$-selective materials.[2−5] Their high performance has been attributed to the interaction between the EO unit and $CO_2$.[6,7] By controlling the crystallinity of the copolymers by changing the content and molecular weight of the ethylene oxide segment and by altering its microstructure by chemical modification, block copolymers with improved properties can be synthesized.[8−12] However, the chemical modification can be expensive or for other reasons not feasible for large scale production of membranes. An important alternative is the simple incorporation of a second phase into existing polymers, which already have high performance. This modification can be done by blending with specific additives, which might be liquids or solids (nanoparticles).[7,12−16]

The addition of polyethylene glycol (PEG) to the poly(amide-*b*-ethylene oxide) copolymer (Pebax) demonstrated that $CO_2$ permeability and selectivity over $H_2$ can be simultaneously increased.[13] This enhancement was attributed to the high $CO_2$ solubility in PEG, but a free volume increase was also taken into consideration because a decrease in density and glass-transition temperature ($T_g$) was observed. Later, the increase in total free volume and fractional free volume was demonstrated for the Pebax/PEG blend.[17]

*Corresponding author. Tel: +494152872403. Fax:+494152872466. E-mail: Wilfredo.Yave.Rios@gkss.de.

Poly(ethylene oxide)−poly(butylene terephthalate) (PEO−PBT) is another material with high $CO_2$ separation performance (known as Polyactive). By controlled addition of PEG into PEO−PBT, polymeric membranes were tailored.[9] High $CO_2$ permeability and high selectivity over $H_2$ and $N_2$ were obtained for the developed membranes. After these two works, we found that the addition of PEG had a limit on the permeability and selectivity improvement. The hydroxyl group of PEG tends to form hydrogen bonding with the ether groups in the copolymer, and thereby the number of free EO units decreases and the $CO_2$ solubility reaches a maximum; consequently, the permeability increase was limited. For increasing the $CO_2$ permeability without affecting the selectivity, other strategies were then considered to increase the total free volume, that is, the static and dynamic free volume of the polymer system, to a much higher extent than that observed for Pebax/PEG blends.[17−19]

PEGs with different end groups such as methyl ether, ethyl ether, vinyl ether, phenyl ether, and so on have almost the same $CO_2$ solubility. Their densities however are different, and some of them have even lower density than PEG, indicating a high free volume. A careful selection of modified PEGs as spacer or filler to be added to the copolymer matrix was expected to increase the total free volume and, consequently, the permeability as well. The spacer or filler should hinder the hydrogen bonding between polymer chains and increase the space between them. At the same time, the glass-transition temperature should decrease (because of the increase in chain mobility and free volume) as well as the crystallinity, leading to higher fractional free volume and enhanced $CO_2$ permeability.[7,17] Besides the effect of solubility diffusion in the polymer bulk, the nanostructured surface morphology of membranes, in the form of a disordered nanofiber- or "mikado"-like structure, seems to influence the separation performance as well.[7]

On the basis of the works mentioned above and others previously reported by other groups,[3,5,20,21] we concluded that

 Published on Web 10/27/2009 

$CO_2$-philic polymer membrane materials should be multiblock copolymers containing high content of EO units as amorphous phase (for high solubility), relatively high free volume (i.e., increased polymer−polymer interchain distance and low cohesive energy), low crystallinity of the hard phase (if possible, completely amorphous and EO units between them), and controlled nanostructure at the surface. Low crystallinity favors the gas transport as well as low glass-transition temperature, which means flexibility of the polymer chains and increased total free volume. When the hard phase (which is commonly considered as impermeable) is less crystalline or amorphous, eventually by including PEO segments into it, it also contributes to the gas transport and to the total permeability value. The nanostructured surface morphology as mikado-like structure results in membranes with large surface-to-volume ratio, and hence it might also have an impact on gas transport properties.[7,22,23]

Here we have developed nanostructured $CO_2$-philic polymer membranes following the idea described above. We blended a commercial multiblock copolymer with two specific polyethylene glycol ethers. The careful selection of PEG−ether as spacer allowed us to tailor the amorphous/crystallinity ratio, the total free volume, the nanostructure of block copolymer blends, and, consequently, the gas transport properties, resulting in membranes with the highest permeability and high $CO_2$ selectivity.

## Experimental Section

**Materials.** Polyactive copolymers from IsoTis OrthoBiologics were used without further purification. The copolymer contains 77 wt % of PEO (1500 g/mol) and 23 wt % of PBT; basic properties of this copolymer can be found elsewhere.[9] The PEG and the functionalized PEGs were purchased from Merck (PEG 200 g/mol), Sigma-Aldrich (PEG−butyl ether 206 g/mol), and Clariant (polyglycol BB 300 g/mol). They had a similar number of EO units ($n = 3-5$) and were used without any purification. Tetrahydrofuran (THF) was used as solvent to prepare the polymer solutions.

**Membrane Preparation and Characterization.** The polymer solutions (3 wt %) were prepared at room temperature for at least 12 h by stirring. The resulting polymer solutions were filtered through a steel filter with pore size 32 $\mu$m (F. Carl Schröter) before membrane preparation. For the blend membranes, PEG and modified PEGs were added to the polymer solution, where the quantity of PEGs was controlled to obtain 40 wt % of PEG with respect to the polymer. The dense film were prepared by casting on a Teflon ring mold; the solvent evaporation was controlled by covering it with a glass dish for 24 h at room temperature. The membrane thicknesses were measured by a digital micrometer; they were between 50 and 100 $\mu$m.

For composite membrane preparation, the obtained polymer solution (3 wt %) was diluted up to 1.0 wt %, and different PEGs were added to obtain a polymer system with 40 wt % of PEG. The composite membranes were prepared by dip-coating. Polyacrylonitrile (PAN) microporous membrane (PAN HVIII) fabricated at GKSS-Forschungszentrum was used as support. After the dip-coating procedure, the membranes were dried under ambient conditions.

We measured the permeabilities of gases at 30 °C by using a pressure increase time-lag apparatus, as reported in ref 9. The feed pressure was 300 mbar for all gases, and the permeate pressure did not exceed 15 mbar. Diffusion coefficients were determined by the time lag method. For fast gases like hydrogen, the error of $D$ is mainly based on the error of the time lag; its error was determined to be $< 0.05$ s. Before the experiments were performed, the sample was dried overnight under vacuum.

A pressure increase test unit designed and built at GKSS was used to measure the permeance of single gases at 30 °C and 1 bar of feed pressure. The permeance values of a membrane with an unknown thickness of the selective layer are called flux ($J$) [l bar$^{-1}$ m$^{-2}$ s$^{-1}$], which can be calculated by using eq 1

$$J = \frac{V \cdot 22,4}{R \cdot T \cdot A \cdot t} \ln\left(\frac{p_F - p_0}{p_F - p_{p(t)}}\right) \quad (1)$$

where $V$ (L) is the permeate volume, $R$ (0.0831 bar l mol$^{-1}$ K$^{-1}$) is the ideal gas constant, $T$ (K) is the temperature, $A$ (m$^2$) is the membrane area, $t$ (s) is the time of measurement, and $p_F$, $p_0$, and $p_{p(t)}$ (bar) are the pressures at the feed, permeate side at beginning, and permeate side at the end of measurement, respectively.

The flow rate of single gases at different pressures (up to 10 bar) and 293 K was tested with a similar device described above, with the difference that fluxes were measured manually by the use of a bubble meter (Bioblock Scientific).

Mixed gas measurements of $CO_2/H_2$ and $CO_2/N_2$ were carried out at feed pressure up to 10 bar and 293 K. Permeate pressure was ~1.1 bar, and the stage-cut (ratio permeate flow to feed flow) during the measurements was $< 1\%$. The feed composition for $CO_2/H_2$ and $CO_2/N_2$ mixtures was 50/50 and 28/72 vol %, respectively.

The compositions of the feed, retentate, and permeate side were analyzed by a gas chromatograph (Variant 3400 with column Chromosorb 107), and the flux of gases was determined by the following equation

$$J_A = \frac{V_{P,A}}{A_m \cdot (f_{R,A} - f_{P,A})} \quad (2)$$

where $V_P$ represents permeate volume flow rate, $A_m$ is the membrane area, and $f_R$ and $f_P$ are fugacities of retentate and permeate. The fugacity was determined by the Redlich−Kwong−Soave equation using Aspen Plus. The area of all membrane samples was 35 cm$^2$.

We characterized the thermal properties of samples in the temperature range from −120 to 250 °C by using a Netzsch (differential scanning calorimeter) DSC 204 calorimeter. The measurements, including baseline determinations, were performed at a scan rate of 10 °C min$^{-1}$, and the experiments were conducted using a nitrogen purge gas stream.

FTIR spectra were obtained on a Bruker EQUINOX 55FTIR spectrometer equipped with attenuated total reflectance (ATR) accessory. All spectra were acquired from 4000 to 550 cm$^{-1}$ under ambient conditions. The number of scans taken was 128 with spectral resolution of 2 cm$^{-1}$.

Wide angle X-ray scattering (WAXS) and small-angle X-ray scattering (SAXS) experiments were performed at the soft condensed matter beamline A2 at HASILAB/DESY. The experiments were done at a fixed wavelength of 0.15 nm and two different sample−detector distances. Synchrotron radiation X-rays were used and detected with a bidimensional MarCCD detector. The calibration of the WAXS region was done with polyethyleneterephthalate (PET), and the calibration of SAXS was done with RTT (rat tendon tail). The circular patterns were integrated using A2Tool (in-house software development).

The resulting morphology and roughness of membrane surface was analyzed by atomic force microscopy (AFM), which was conducted by a NanoScope IIIa (Digital Instruments) in constant force mode at room temperature with the dried membrane sample. The thickness of composite membranes was analyzed by scanning electron microscopy (SEM). The SEM analyses were carried out with a LEO 1550 VP Gemini (ZEISS) microscope.

## Results and Discussion

**Gas Transport Properties.** It is known that polymeric materials based on PEG or PEO are highly selective to $CO_2$. They present high permeability because of the high $CO_2$ solubility, which is a result of the favorable interaction

**Table 1. $CO_2$ Permeability and Selectivity Over $H_2$, $N_2$, and $CH_4$ for PEO−PBT Dense Membranes with 40 wt % of Different PEG Spacers (BE: Butyl Ether, DBE: Dibutyl Ether)**

| sample | $CO_2$ permeability [barrer][a] | $CO_2/H_2$ | $CO_2/N_2$ | $CO_2/CH_4$ |
|---|---|---|---|---|
| PEO−PBT | 150 | 10.3 | 51.5 | 16.8 |
| PEO−PBT + PEG | 208 | 11.6 | 48.7 | 15.8 |
| PEO−PBT + PEG−BE | 400 | 11.8 | 50.1 | 12.5 |
| PEO−PBT + PEG−DBE | 750 | 12.4 | 40.0 | 11.2 |

[a] [barrer] = $1 \times 10^{-10}$ ($cm^3$ (STP) cm $cm^{-2}$ $s^{-1}$ cm $Hg^{-1}$).

between ethylene oxide units and $CO_2$.[2,3] Nevertheless, the $CO_2$ solubility selectivity can be increased only up to a limit by adding PEG with usual OH terminal groups.

To increase the solubility selectivity as well as the diffusivity selectivity, a specific PEG with other terminal group was selected as spacer. This modified PEG increases the $CO_2$ solubility in the membrane, as observed for the conventional PEG, but simultaneously, the diffusivity is enhanced (discussed later). The permeability is five-fold increased (Table 1), going from 150 barrer (pristine copolymer) to 750 barrer (blend membrane). The modified PEGs have butyl end groups. They were chosen with the expectation that the butyl end groups could favorably interact with the butylene segment of the butylene terephthalate block because of structural similarity (hydrophobic segments). The crystalline phase of PBT could then be more efficiently destroyed by PEG−butyl ether molecules at the same time; the distance between polymeric chains (free volume) in this phase could be increased.

Table 1 presents the values of $CO_2$ permeability and selectivity over $H_2$, $N_2$, and $CH_4$ for the pristine copolymer membrane and for blends with two different modified PEGs as spacer (PEG−butyl ether (PEG−BE) and PEG−dibutyl ether (PEG−DBE)). Blends with nonmodified PEG are also included for comparison. Other PEG−ethers, which enhanced the permeability of Pebax membranes, were also checked to see how they behave as spacer and how the ether end group influences the membrane performance (Supporting Information).

The $CO_2$ permeability is substantially increased by the addition of PEG with end groups different than hydroxyl. On one hand, when hydroxyl-terminated PEG is used as an additive, the $CO_2$ permeability is increased by only 30% in relation to the pristine PEO−PBT, and this increase is mostly due to the increase in $CO_2$ solubility.[3,13,24] On the other hand, it is clear that in particular the presence of butyl end groups in the PEG chain greatly enhances the permeability. The $CO_2$ permeability and $CO_2/H_2$ selectivity are higher than those of pristine PEO−PBT. However, the $CO_2/N_2$ and $CO_2/CH_4$ selectivity in these polymeric systems slightly decreased. For PEO−PBT/PEG−DBE membranes, the $CO_2/N_2$ and $CO_2/CH_4$ selectivity values are lower than those for other blends. As can be seen later by other evidence, it is possible that PEG−DBE partially separates from the PEO−PBT copolymer, forming a microphase through which $CO_2$ and $CH_4$ transport could preferentially occur. Although a phase separation could have occurred, which will also be discussed later, it must be on the nanometer scale because the films were completely transparent and robust (Supporting Information).

The incorporation of PEG−DBE improved the $CO_2$ solubility of the membranes from (2.50 to 3.70) $\times 10^{-2}$ $cm^3$ (STP) $cm^{-3}$ cm $Hg^{-1}$ (Table 2), which is due to the increased EO content. The relative $CO_2$ diffusivity (ratio between the diffusivities of the blend and pristine copolymer) is greatly

**Table 2. Diffusivity and Solubility of Different Gases for PEO−PBT Dense Membranes and Blends with Different PEG Spacers (40 wt % of Spacer)[a]**

| Sample | $CO_2$ | | $H_2$ | | $N_2$ | | $CH_4$ | |
|---|---|---|---|---|---|---|---|---|
| | *D* | *S* | *D* | *S* | *D* | *S* | *D* | *S* |
| PEO−PBT | 0.62 | 250 | 4.4 | 3.3 | 0.9 | 3.3 | 0.5 | 18 |
| PEO−PBT + PEG | 0.76 | 280 | 5.0 | 3.4 | 1.0 | 4.2 | 0.7 | 20 |
| PEO−PBT + PEG−BE | 1.36 | 270 | 5.4 | 5.0 | 2.0 | 4.6 | 1.2 | 20 |
| PEO−PBT + PEG−DBE | 2.03 | 370 | 9.6 | 5.9 | 2.7 | 8.2 | 2.0 | 37 |

[a] $D \times 10^7$ ($cm^2$ $s^{-1}$) and $S \times 10^4$ ($cm^3$ (STP) $cm^{-3}$ cm $Hg^{-1}$).

increased, confirming that the total free volume of the polymeric system has been increased. Because of the free volume increase, the $N_2$ and $CH_4$ relative diffusivity is increased in the same range as that for $CO_2$, the solubility of these two gases is increased more than that of $CO_2$, and, as consequence, the $CO_2/N_2$ and $CO_2/CH_4$ selectivity decreased, as shown in Table 1. The high $CO_2$ permeability (750 barrer), the high $CO_2/H_2$ selectivity (12.4), and the reasonable $CO_2/N_2$ selectivity (40.0) make this membrane material promising for applications involving these gas mixtures.

By the addition of the DBE-terminated PEG, which act as a plasticizer or even as a spacer, the $CO_2/H_2$ diffusivity selectivity was increased by almost 50%, whereas the solubility selectivity decreased (~25%) or remained constant (Supporting Information). The PEG−DBE chains can be positioned between PEO and PBT segments, inducing higher chain motion due to the increased free volume. Simultaneously, because of the high concentration of ethylene oxide units due to PEG−DBE addition, the $CO_2$ solubility is enhanced (Table 2). The presence of butyl groups at the end of the PEG chain does not favor hydrogen bonding (weak cohesive energy), leaving more EO units free to interact with $CO_2$. Altogether, these facts contributed to the improved $CO_2$ permeability (five-fold) and $CO_2/H_2$ selectivity (~20%).

**Thermal Properties.** Thermal properties and the crystallinity of polymeric membranes have been correlated to the gas transport capabilities.[25,26] Figure 1 shows the first (a) and second (b) scan thermograms obtained by differential scanning calorimetry (DSC). The curves obtained in the first scan for PEO−PBT (pristine) as well as for blends with PEG and PEG−BE present two peaks corresponding to the PEO and PBT melting temperatures. For PEO−PBT/PEG−DBE, besides the peaks mentioned above, an additional one, which could correspond to a separated microphase of PEG−DBE (−48 °C), was clearly identified. At the same temperature, a smooth transition is also seen for the blend with PEG−BE, however, with very low intensity. All of these peaks (from −100 to 200 °C) confirm the presence of different crystalline phases in the as-cast membranes. The glass-transition temperature corresponding to the PEO block, detected for the pristine copolymer at about −50 °C, is shifted for the blends to lower temperatures, confirming that the total free volume is increased.[17]

The melting temperature of the PEO phase (peak at 19 °C) for pristine PEO−PBT is shifted to lower values when PEGs (OH- and butyl-terminated) are added (Figure 1a). A slight shifting is also detected for blends with dibutyl-terminated PEG. The crystallinity of the PEO phase is lower for blends with PEG−BE and PEG−DBE than for the pristine polymer (Supporting Information), which supports the fact that the $CO_2$ permeability increases because of the increase in the amorphous phase content. For the blend with OH-terminated PEG, an increase in crystallinity was observed. The

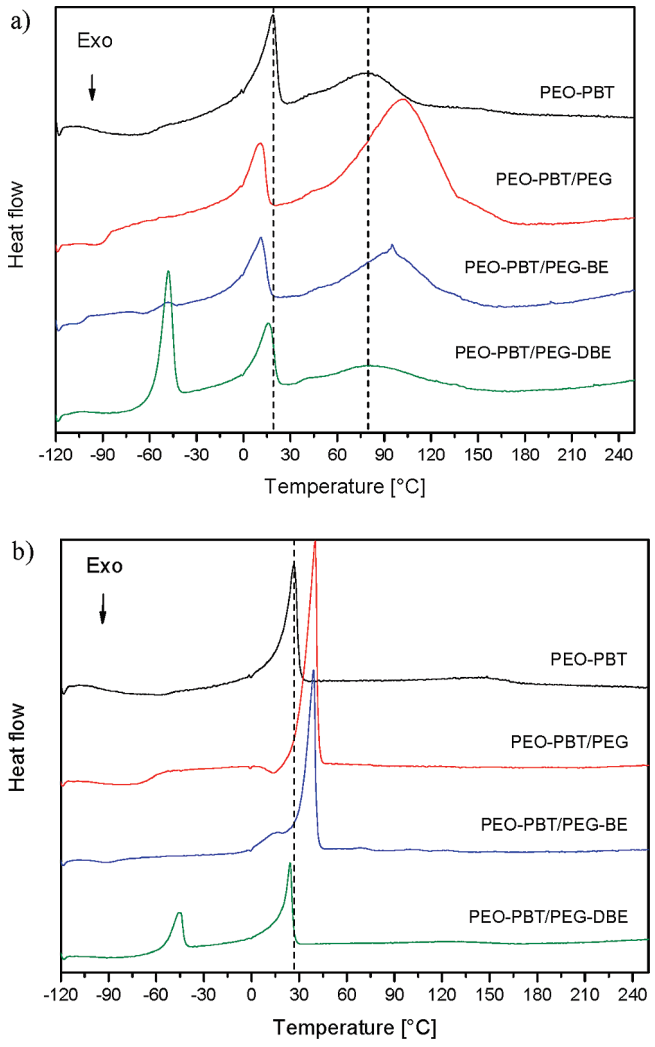


**Figure 1.** DSC thermograms of nanostructured blend membranes: (a) first and (b) second scan (10 °C $min^{-1}$).

PEG additive induces the packing of EO segments of the copolymer chain, forming additional hydrogen bonds. Although the PEG contributes to a slightly higher $CO_2$ solubility (Table 2) because of the higher content of EO units, the higher crystallinity hinders a substantial increase in permeability.

A peak around 80−100 °C can be observed for all membranes in the first DSC scan. The peak might be related to the PBT phase. However, the PBT melting temperature has been reported in the literature between 110 and 210 °C.[8−10] In the second scan (Figure 1b), this peak is not observed; only a small peak around 150 °C can be seen for the pristine copolymer, corresponding to the melting of PBT crystallites. A shoulder in the same temperature region can be seen in the first scan, at least for blends with OH-terminated PEG.

The peak around 80−100 °C probably reflects an ordered structure that is rich in butylene terephtalate, which has been ordered during casting from solution. In the presence of solvent, the low viscosity facilitates the polymer organization. At the same time, very small amounts of solvent might also interact with the polymer, inducing an ordered structure that disappears after the first scan, and thus in the second scan, no peak is observed.

The PEO melting temperature in the second scan is shifted to higher values, becoming very sharp with increased integrated area and consequently higher crystallinity. After heating and at the applied cooling rate, the crystallization of PEO is favored.

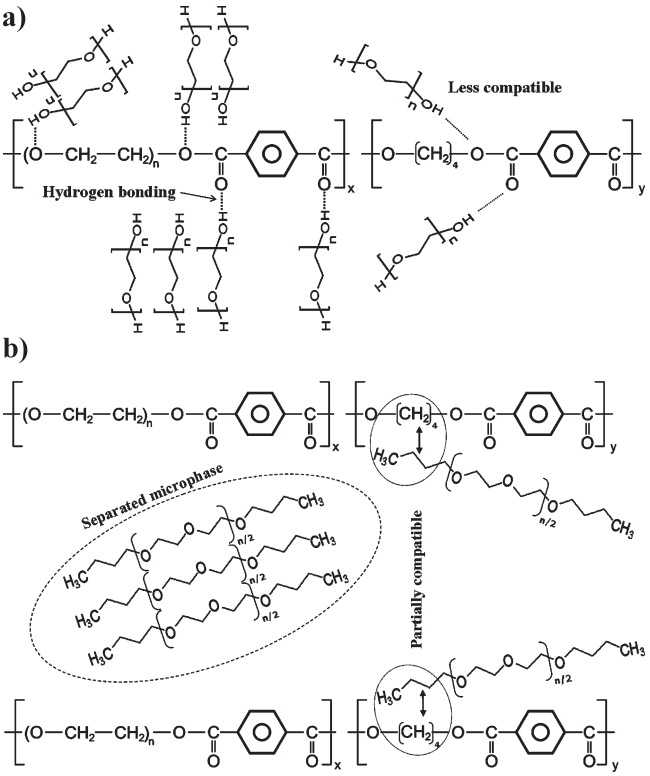


**Figure 2.** Schematic representation of PEO−PBT/PEG (a) and PEO−PBT/PEG−DBE (b).

The presence of two melting temperatures below 20 °C for the PEO−PBT/PEG−DBE blend as well as the near absence of temperature shift for the peaks around 25 and 80 °C (compared to the pristine copolymer) indicates a segregation of the additive, forming a separated phase, which is large enough to be characterized by DSC. With this information and by taking into account the high crystallinity of PEO−PBT/PEG, a schematic representation can be proposed in Figure 2 (to understand the structure of blends).

The PEG induces the organization of PEO segments in the copolymer because of the strong hydrogen bonding between the hydroxyl group of PEG and ether groups of the PEO−PBT copolymer (Figure 2a). This ordering increases the crystallinity and reduces the number of EO units available for interaction with $CO_2$; therefore, the $CO_2$ permeability increase is limited. Nevertheless, when PEG−DBE is used as an additive, it works as a spacer because of the butyl end group. The butyl end group hinders the hydrogen bonding and is somewhat compatible with PBT because of butylene segments in this phase. If PEG−DBE is dispersed in the PBT phase, then the $CO_2$-philic character of this phase is improved, and the interchain distance could also be increased (Figure 2b), which greatly enhanced the $CO_2$ permeability.

The hydrogen bonding has been analyzed by Fourier transfer infrared (FTIR) spectra (Supporting Information). The bands at 2866 (not depicted), 1714, 1272, and 727 $cm^{-1}$ were assigned to PEO−PBT.[27] All spectra are similar, and only the small band at ~1208 $cm^{-1}$ is shifted to higher frequencies (1200 $cm^{-1}$) for the PEO−PBT/PEG−DBE blend. This shifting could indicate that the hydrogen bonding in this blend is weak, which would support the hypothesis that less hydrogen bonding occurs in the presence of PEG−DBE. Moreover, the intensity of the bands (1714, 1272, and

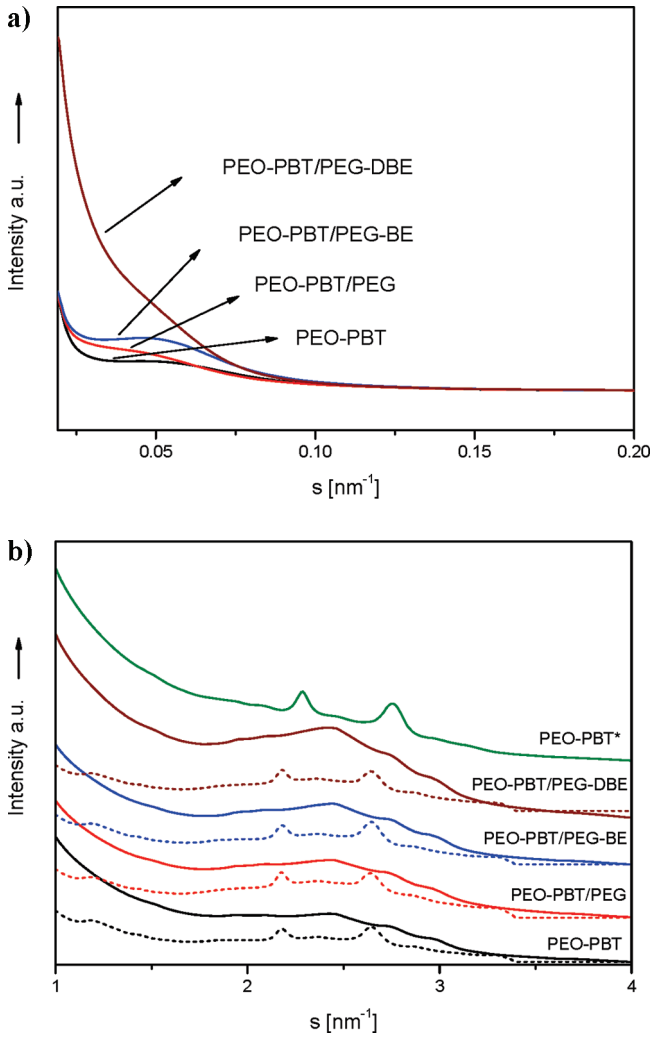


**Figure 3.** X-ray diffractograms of PEO−PBT and its blends with PEG terminated with different groups. (a) Small angle X-ray scattering (SAXS) at room temperature and (b) Wide angle X-ray scattering (WAXS); the solid line data are at room temperature and the dashed lines correspond to those at 0 °C.

1252 $cm^{-1}$) decreased for all blends because of dilution in the presence of additives.

**Scattering Characterization.** No macrostructure formation was observed by small-angle X-ray scattering (SAXS) (patterns shown in Figure 3a), and the membranes were amorphous.

The SAXS patterns show that the blend containing PEG−DBE is quite more distinct than the others. The higher scattering intensity at low "*s*" values suggests the occurrence of larger nanodomains (microphase separation). The ordered structures of the PBT phase surrounded by the PEO amorphous phase (observed by DSC as a transition around 80−100 °C) could be responsible for the scattering maximum around 0.05 $nm^{-1}$. These ordered domains in pristine copolymer have a characteristic dimension of ca. 20 nm, and for samples containing PEG−BE, this dimension is 22 nm. For curves corresponding to the PEO−PBT/PEG and PEO−PBT/PEG−DBE, the maximum at this point can practically not be seen, although the phase transition was evident in DSC measurements.

The wide-angle X-ray scattering (WAXS) results confirmed that the samples are completely amorphous at room temperature (Figure 3b, solid lines), the X-ray diffraction patterns are broad and without any indication or recognizable pattern. The diffuse halo at ~2.5 $nm^{-1}$ corresponds to the PBT hard and PEO soft phases.[28−30] The characteristic peaks of PBT crystallite are expected in this region, and according to the literature, the WAXS for PBT homopolymer is characterized by five peaks.[28,29] A sample of PEO−PBT (pristine copolymer) with higher crystallinity in the PEO phase (42%) is also included in Figure 3b as PEO−PBT*, and the patterns for this copolymer display two intense peaks. These two characteristic peaks correspond to the PEO crystallites, which indicate its high crystallinity.[30]

The PEO−PBT copolymer used in the membrane preparation is in fact less crystalline and is characterized by a more diffuse scattering curve, which agrees with its more amorphous character. The diffuse halo is slightly shifted to lower "*s*" values when PEO−PBT is blended with PEG−DBE, and thus this shifting can be related to the increase in interchain distance in the amorphous phase due to the PEG−DBE presence. This agrees with the increased gas diffusivity. (See Table 2.) As we discussed above, the small PEG−DBE molecules can be positioned between polymer chains, which create a $CO_2$-philic polymer with higher chain motion and higher total free volume. Great changes in *d*-spacing are not observed because PEG and PEO are analogous, independently if polymer−polymer chains or polymer−PEG are considered.

At lower temperatures (0 °C), the blends and the pristine PEO−PBT exhibited the two characteristic peaks of PEO crystallites (Figure 3b, dashed lines). These peaks are slightly shifted to lower "*s*" values compared with PEO−PBT*, and they are therefore associated with the increase in lattice space.

**Morphological Characterization.** The assumption based on DSC and X-ray analysis, that is, the presence of an ordered structure of PBT and phase separation of PEG−DBE and PEO−PBT, is supported by atomic force microscopy (AFM) (Figure 4). Representative AFM phase images of the surface of PEO−PBT membranes clearly show a microphase-separated nanostructure, with PBT hard segment (nanofibril-like) embedded into an amorphous PEO soft segment (Figure 4a). For the PEO−PBT/PEG blend, the nanofibril structures are even more evident, dispersed in larger and more clearly separated domains of the other phase (Figure 4b), corresponding to the ordered PBT hard segment surrounded by the EO rich phase with high content of low-molecular-weight PEG. As discussed above, the PEG could form hydrogen bonding with the ether group from EO units; thereby, the molecular organization is high, and it can increase the crystallinity of the sample.

Figure 4c shows the surface of the PEO−PBT/PEG−BE blend. The nanostructure of this sample is more similar to that of Figure 4a. For this sample, the crystallinity was lower than that of the pristine copolymer, and the PEO phase is more amorphous, just surrounding the well-structured butylene-teraphtalate-rich nanofibrils. The surface of the PEO−PBT/PEG−DBE membrane presents three phases (Figure 4d), two phases similar to those observed in previous Figures and an additional phase that corresponds to the PEG−DBE-separated phase. The PEG−DBE-separated phases are larger and can be seen as islands or hills (brighter areas). In the DSC thermogram, they are responsible for the melting temperature observed at −48 °C.

Surface roughness profiles (qualitative views in three directions) of PEO−PBT and its blends were also analyzed (Supporting Information). For PEO−PBT/PEG−DBE, the $R_{max}$ (maximum vertical distance between the highest and lowest data points in the image) value was detected to be ~45 nm (the highest), and for the blend containing just PEG,

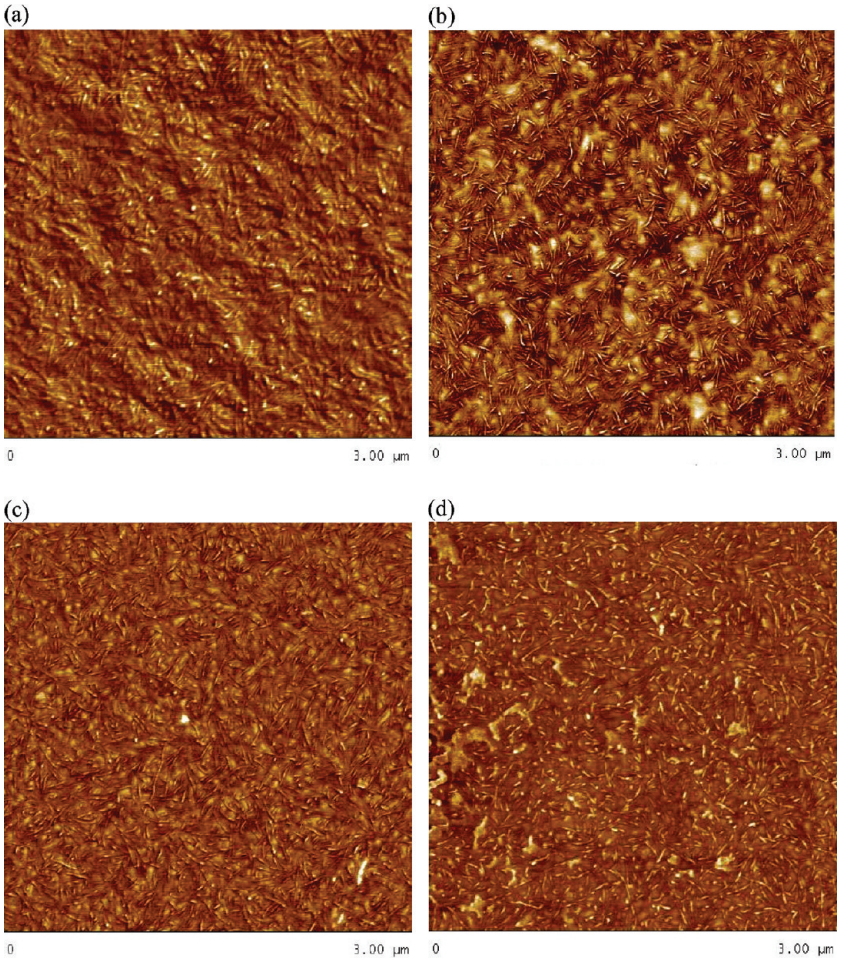


**Figure 4.** Atomic force microscopy (AFM) phase images of nanostructured membrane surface of: (a) PEO−PBT, (b) PEO−PBT/PEG, (c) PEO−PBT/PEG−BE, and (d) PEO−PBT/PEG−DBE.

it was ~27 nm, which was the lowest. For the PEO−PBT pristine copolymer and for the blend with PEG−BE, similar values, 34 and 36 nm, respectively, were registered. Rough surfaces mean high effective surface area (larger surface-to-volume ratio); thereby, the $CO_2$ molecules, which first are absorbed on the surface and then dissolve in the polymer, can easily further permeate through the membrane bulk, which has increased free volume.[17]

The contact angle of water on these surfaces was 80, 50, 60, and 50° for pristine PEO−PBT and blends with PEG, PEG−BE, and PEG−DBE, respectively. The contact angle of pristine copolymer is high (80°), and it is generally decreased by PEG addition. The interesting point is that despite the surface roughness of PEO−PBT/PEG−DBE ($R_{max} \approx 45$ nm), the contact angle is low and typical for a hydrophilic surface, and hence rough surfaces and lower contact angle (hydrophilic surface) produced a highly $CO_2$-permeable material ($CO_2$-philic).

These results show that the addition of PEG−DBE into the PEO−PBT produced at the same time a highly hydrophilic and rough surface, resulting in membranes with high $CO_2$ separation performance.

**Thin Film Composite Membrane.** The developed $CO_2$-philic material described above has been manufactured into thin film composite membranes. They were prepared from a polymer solution (1 wt %) on two supports, polyacrylonitrile (PAN) microporous membrane and PAN coated with a layer of poly(dimethylsiloxane) (PAN−PDMS). The measured $CO_2$ fluxes through the composite membranes are extremely high, and the selectivities are still attractive (Table 3), which make them very attractive for industrial application.

Table 3 presents the $CO_2$ flux and selectivity over $H_2$ and $N_2$ of thin film composite membranes for PEO−PBT pristine polymer and PEO−PBT/PEG−DBE blend. As expected, in all cases, the blends (bold data) have higher $CO_2$ fluxes (>40%) than the pristine copolymer membrane (first group data). Only a slight selectivity decrease was detected compared with the corresponding pristine copolymer. The application of an additional PDMS gutter layer enhanced the flux by 30%.

The up-scaled $CO_2$-philic membrane produced on large scale (second and third group data, Table 3) showed that the $CO_2$ fluxes measured under different conditions are similar. In all cases, typical behavior of rubbery-like membranes was observed; the $CO_2$ flux in gas mixtures is almost the same, but the selectivity dropped at higher pressure. This behavior is typical as a result of plasticization.

From the mathematical relation (permeability = flux * thickness), the estimated thickness for PEO−PBT thin film on PAN-support is ~500 nm. The experimental value estimated from scanning electron microscope (SEM) image was ~150 nm (Figure 5d). This difference is due to the polymer solution penetration into the pores of the support. The thickness experimentally observed by SEM is only the top layer; the penetration of the solution leads to an additional equivalent thickness of 350 nm. The use of PAN-PDMS support hinders the polymer solution penetration,

**Table 3. $CO_2$ Flux and Selectivity over $H_2$ and $N_2$ for PEO−PBT Composite Membranes under Different Operating Conditions (Blends with 40 wt % of PEG−DBE Spacers)**

| sample (support) | pressure (bar)[a] | $CO_2$ flux ($m^3\ m^{-2}\ h^{-1}\ bar^{-1}$) | α $CO_2/H_2$ | α $CO_2/N_2$ |
|---|---|---|---|---|
| | | Single Gas | | |
| PEO−PBT (PAN) | 1 | 0.8 | 10 | 55 |
| PEO−PBT/PEG−DBE (PAN) | 1 | 1.4 | 9 | 50 |
| PEO−PBT (PAN−PDMS) | 1 | 1.1 | 10 | 50 |
| PEO−PBT/PEG−DBE (PAN−PDMS) | 1 | 1.9 | 10 | 40 |
| | | Single Gas at High Pressure | | |
| PEO−PBT/PEG−DBE (PAN−PDMS) | 5 | 2.1 | 15 | 44 |
| | 10 | 2.4 | 16 | 46 |
| | | Mixed Gas at High Pressure | | |
| PEO−PBT/PEG−DBE (PAN−PDMS) | 5 | 2.2 | | 40 |
| | 10 | 1.9 | | 33 |
| | 5 | 2.4 | 8 | |
| | 10 | 2.5 | 8 | |

[a] Feed pressure.

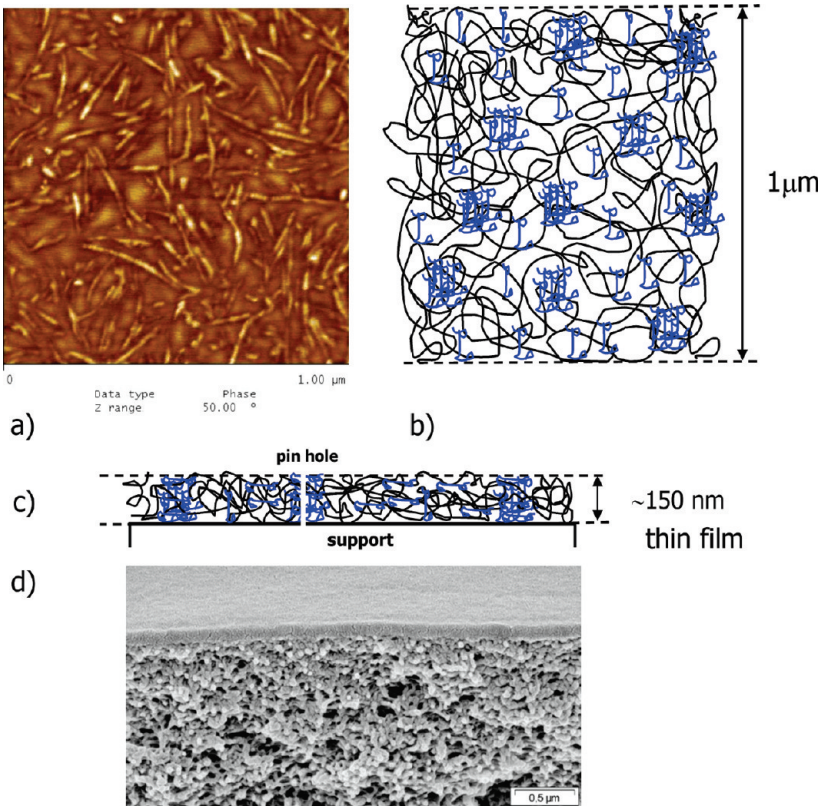


**Figure 5.** (a) AFM phase image of PEO−PBT/PEG−DBE blend, (b) schematic representation of AFM image (the blue color represents the PEG−DBE separated phase), (c) schematic representation of thin film with a defect or pinhole, and (d) scanning electron microscopy (SEM) of pristine copolymer (composite membrane on PAN support).

and the flux has been increased because of thickness reduction.

The islands of PEG−DBE-separated phase (Figure 5a,b) may probably have sizes similar to the selective thin layer thickness (membranes prepared on PAN-PDMS support), and they could create a few defects or pin holes in the thin film (Figure 5c). Nevertheless, when the composite membrane is prepared directly on PAN support, the polymer solution can partially drain through the pores because of the low viscosity of PEG−DBE with low molecular weight. The effective selective layer is therefore thicker, the defects or pinholes can be avoided, and higher $CO_2/N_2$ selectivity can be achieved.

## Conclusions

Highly $CO_2$-philic polymer membranes based on commercial PEO−PBT copolymer and PEG−DBE were developed. By careful selection of PEG−ether as spacer, the $CO_2$ permeability of membranes was five-fold increased, and the selectivity values over $H_2$ and $N_2$ were similar to those of the pristine copolymer. The increase in permeability was mainly assigned to the ethylene oxide ($CO_2$-philic character) and total free volume increase in the polymer matrix (increased polymer−polymer interchain distance). The $CO_2$ diffusivity selectivity enhancement has been mainly attributed to the $CO_2$-philic surface, to a slight increase in the total free volume (increased dynamic free volume due to the chain motion), and to the microphase separation of PEG−DBE.

The composite membrane prepared from this $CO_2$-philic polymer system presented extremely high $CO_2$ flux in gas mixtures (up to 2.5 $m^3$ (STP) $m^{-2}$ $h^{-1}$ $bar^{-1}$), and hence it has potential application for $CO_2$ capture. However, studies concerning the stability of thin film composite and its performance under different operating conditions must be carried out (the present work is only devoted to the design of $CO_2$-philic polymeric membrane material); in particular, the occurrence of defects during its performance on long-term must be studied.

**Acknowledgment.** We thank Sabrina Bolmer for the AFM images, Karen Prause for the SEM microphotograph, Silvio Neumann for DSC measurements and André Rothkirch for A2Tool. We also thank Jan Wind and Holger Pingel for preparation of the support membranes. The work was supported by the Helmholtz-Alliance MemBrain project (Gas separation membranes for Zero-emission Fossil Power Plant).

**Supporting Information Available:** Additional information of permeability, solubility, and diffusivity as well as some images of roughness profile (AFM images). This material is available free of charge via the Internet at http://pubs.acs.org.

## References and Notes

(1) Lackner, K. S. *Science* **2003**, *30*, 1677–1678.
(2) Yoshino, M.; Kita, H.; Okamoto, K.-I.; Tabuchi, M.; Sakai, T. *Trans. Mater. Res. Soc. Jpn.* **2002**, *27*, 419–421.
(3) Lin, H.; Freeman, B. D. *J. Mol. Struct.* **2005**, *739*, 57–74.
(4) Blume, I.; Pinnau, I. U.S. Patent 4,963,165 , **1990**.
(5) Sarbu, T.; Styranec, T.; Beckmann, E. J. *Nature* **2000**, *405*, 165–168.
(6) Lin, H.; Wagner, E.; Freeman, B. D.; Toy, L. G.; Gupta, R. P. *Science* **2006**, *311*, 639–642.
(7) Yave, W.; Car, A.; Peinemann, K.-V. *J. Membr. Sci.*, submitted.
(8) Deschamps, A. A.; Grijpma, D. W.; Feijen, J. *Polymer* **2001**, *42*, 9335–9345.
(9) Car, A.; Stropnik, C.; Yave, W.; Peinemann, K.-V. *Adv. Funct. Mater.* **2008**, *18*, 2815–2823.
(10) Metz, S. J.; Mulder, M. H. V.; Wessling, M. *Macromolecules* **2004**, *37*, 4590–4597.
(11) Arnold, M. E.; Nagai, K.; Freeman, B. D.; Spontak, R. J.; Betts, D. E.; DeSimone, J. M.; Pinau, I. *Macromolecules* **2001**, *34*, 5611–5619.
(12) Patel, N. P.; Miller, A. C.; Spontak, J. *Adv. Funct. Mater.* **2004**, *14*, 699–707.
(13) Car, A.; Stropnik, C.; Yave, W.; Peinemann, K.-V. *J. Membr. Sci.* **2008**, *307*, 88–95.
(14) Novel Membranes for $CO_2$ Removal, **2009**. DOE - National Energy Technology Laboratory Web site. http://www.netl.doe.gov/publications/factsheets/rd/R&D047.pdf.
(15) Chung, T.-S.; Jiang, L. Y.; Kulprathipanja, S. *Prog. Polym. Sci.* **2007**, *32*, 483–507.
(16) Yave, W.; Shishatskiy, S.; Abetz, V.; Matson, S.; Litvinova, E.; Khotimskiy, V.; Peinemann, K.-V. *Macromol. Chem. Phys.* **2007**, *208*, 2412–2418.
(17) Yave, W.; Car, A.; Peinemann, K.-V.; Shaikh, M. Q.; Rätzke, K.; Faupel, F. *J. Membr. Sci.* **2009**, *339*, 177–183.
(18) Forsyth, M.; Meakin, P.; MacFarlane, D. R.; Hill, A. J. *J. Phys.: Condens. Matter* **1995**, *7*, 7601–7617.
(19) Kobayashi, Y.; Haraya, K.; Kamiya, Y.; Hattori, S. *Bull. Chem. Soc. Jpn.* **1992**, *65*, 160–163.
(20) Freeman, B. D.; Pinnau, I. *Trends Polym. Sci.* **1997**, *5*, 167–173.
(21) Raveendran, P.; Wallen, S. L. *J. Am. Chem. Soc.* **2002**, *124*, 12590–12599.
(22) Gronda, A. M.; Buechel, S.; Cussler, E. L. *J. Membr. Sci.* **2000**, *165*, 177–187.
(23) Yuan, J.; Liu, X.; Akbulut, O.; Hu, J.; Suib, S. L.; Kong, J.; Stellacci, F. *Nat. Nanotechnol.* **2008**, *3*, 332–336.
(24) Henni, A.; Tontiwachwuthikul, P.; Chakma, A. *Can. J. Chem. Eng.* **2005**, *83*, 358–362.
(25) Van Krevelen, D. W. *Properties of Polymers Part IV: Transport Properties of Polymers*; Elsevier Scientific Publishing Company: Amsterdam, The Netherlands, 1990.
(26) Mulder, M. *Basic Principles of Membrane Technology*; Springer-Verlag: New York, 1996.
(27) Du, C.; Klasens, P.; Haan, R. E.; Bezemer, J.; Cui, F. Z.; de Groot, K.; Layrolle, P. *J. Biomed. Mater. Res.* **2002**, *59*, 535–546.
(28) Alter, U.; Bonart, R. *Colloid Polym. Sci.* **1976**, *254*, 348–357.
(29) Prado, L. A. S. A.; Kwiatkowska M.; Funari, S. S.; Roslaniec, Y.; Broya, G., Schulte, K. *Annual Report HASYLAB at DESY*. http://hasyweb.desy.de/science/annual_reports/2006_report/part1/contrib/46/18037.pdf.
(30) Mohd Nasir, N. F.; Raha, M. G.; Kadri, N. A.; Sahidan, S. I.; Rampado, M.; Azlan, C. A. *Am. J. Biochem. Biotechnol.* **2006**, *2*, 175–179.